THE JOURNAL OF PHYSICAL CHEMISTRY C

Article

pubs.acs.org/JPCC

Cage Effect in Poly(alkyl methacrylate) Thin Films Studied by Nile Red Single Molecule Fluorescence Spectroscopy

Beatriz Araoz,[†] Daniela Täuber,[‡] Christian von Borczyskowski,*[,‡] and Pedro F. Aramendía*[,†]

[†]INQUIMAE and Departamento de Química Inorgánica, Analítica y Química Física, Facultad de Ciencias Exactas y Naturales, Universidad de Buenos Aires, Pabellón 2, Ciudad Universitaria, C1428EHA, Buenos Aires

[‡]Optical Spectroscopy and Molecular Physics Group, Institute of Physics, Chemnitz University of Technology, D-09107 Chemnitz, Germany

Supporting Information

ABSTRACT: Interactions in a probe−polymer cage were monitored by spectral fluctuations in the emission spectroscopy of single molecules of Nile Red in poly(alkyl methacrylate) thin films (25−200 nm) in the 278−323 K temperature range. Three types of emission spectra were identified. The highest emission energy spectra show small amplitude fluctuations and a very low probability of changing their spectral emission features. On the other hand, the other two types of emission profiles exchange more frequently. The fluctuations are analyzed by the complementary cumulative distribution function of spectral emission energy difference between successive spectra in a time trace. The fluctuations show three components: two of them with zero mean average and distinctly different standard deviations and a third component with much lower frequency and an amplitude absolute value of 0.13−0.15 eV. This amplitude is the same in all conditions, pointing to a common feature of the probe−polymer cage as responsible for their presence: complex cage rearrangements, involving the carbonyl side chain of the polymer as the common actor are postulated to be the cause of these spectral fluctuations in the time range of seconds.

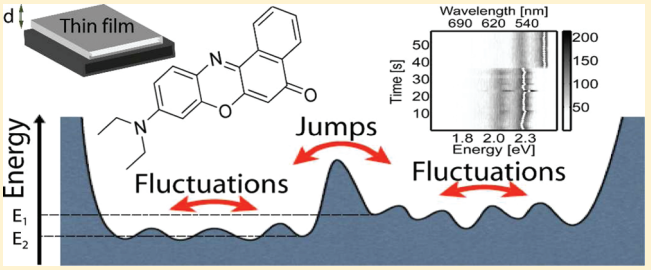

INTRODUCTION

Thin polymer films are often used in organic light-emitting diodes, for recording materials, such as surface relief gratings,[1] or for mechanical actuators[2,3] (photomechanical effect); amorphous polymers are loaded with spectroscopically active dye molecules that turn the system functional upon light stimulus. For many of these applications dyes are embedded in the polymer matrix. The dye location depends on the probe−polymer as well as on the polymer−polymer interactions. The dye location defines a polymer cage as a cavity in the polymer matrix, with flexible walls and variable polarity, with the possibility to accommodate the dye. In a glassy polymer, the probe−polymer cage is both heterogeneous in space and fluctuating in time.[4−6] The heterogeneity in space is related to different molecular environments within the macromolecular framework. The heterogeneity in time is related to temporal fluctuations of probe−polymer conformations. The observed properties of a probe in a polymer environment can thus change from a broad heterogeneous distribution among the different cages, caused by a frozen environment in the time scale of observation, to a homogeneous regime caused by fast averaging of the environment. At the microscopic level, this change in mobility affects dye−polymer interactions and the photochemistry of the dye. Questions related to the spread of behaviors can be studied by bulk measurements and the application of models that retrieve the dynamic distribution. But the time behavior of single dye−polymer cages can only be studied at the single molecule level. Single molecule fluorescence spectroscopy is an ideal technique to study local events and monitor microheterogeneity.[7,8] It has been widely applied to polymer films when doped with medium-sensitive dyes, as reported and summarized in recent reviews.[9−13] Basic questions such as distinguishing between spatial and temporal heterogeneity, the distribution of spectral or kinetic behaviors, or the time persistence of the local fluctuations are topics specially suited to single molecule studies.

Medium-sensitive dyes are used as reporters of microenvironment to monitor this heterogeneity, either statically (solvatochromism)[14] or dynamically (fluorescence lifetime, fluorescence anisotropy, kinetics of photoproduced metastable states).[7,15−18] Nile Red (NR) is an oxazine dye that has been broadly used to monitor events in polymer films[19−27] due to its high emission quantum yield and its strong sensitivity to changes in polarity and in rigidity of the medium, as evidenced by a positive solvatochromic effect.

In this work, we report on single molecule fluorescence emission spectra of NR in polymer films of poly(alkyl methacrylate) of different alkyl chain length (*n*-butyl, PBMA;

Received: January 12, 2012
Revised: March 6, 2012
Published: March 9, 2012

dx.doi.org/10.1021/jp3004097 | *J. Phys. Chem. C* 2012, 116, 7573−7580

n-propyl, PPMA; and methyl, PMMA), of different film thickness (25 or 200 nm), and at different temperature. PPMA (T_g = 305 K) and PBMA (T_g = 298 K) were both investigated below, at about, and clearly above T_g. In PMMA, temperatures at and above T_g (388 K) were experimentally not accessible. This polymer thus serves as a reference of a rigid environment. Spectroscopy clearly shows spatial heterogeneity by differences in spectral distribution, but also heterogeneity in temporal behavior by changes in the emission spectral distribution.

EXPERIMENTAL METHODS

Sample Preparation. 7-Diethylamino-3,4-benzophenoxazine-2-ona (Nile Red, NR) was purchased from Bio Chemika (Sigma for fluorescence). PMMA (M_w = 350.000, T_g = 388 K) and PBMA (M_w = 337.000, T_g = 298 K), from Sigma Aldrich, and PPMA (M_w = 150.000, T_g = 305 K), from Scientific Polymer, were used as received (molecular structures are given in Scheme 1). Polymer solutions were prepared in toluene

Scheme 1. Structures of Dye (Nile Red) and Polymers (R_1, PMMA; R_2, PPMA; R_3, PBMA)

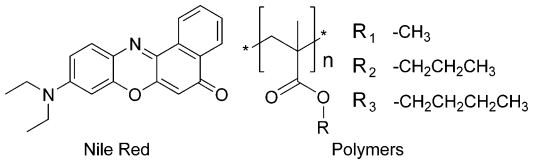

(Aldrich, spectroscopic grade) at different concentration and doped with NR. Thin polymer films were obtained by spin-coating the solution onto a rigorously cleaned silicon substrate, with a 70 nm grown SiO_2 layer to avoid fluorescence quenching. They were dried in vacuum at 323 K for 12 h. The thickness of the spin-coated films was regulated by the concentration of the polymer solutions (0.25 and 2.0% w/w) which were deposited at 3000 rpm. Films of 200 and 25 nm were prepared and characterized by ellipsometry. The thickness of the films was measured using a variable angle ellipsometer (VASE, J.A. Woollam Co., Inc., covering a spectral range from 0.73 to 5 eV). Dye concentration used was at the picomolar level in relation to the polymer concentration to ensure not more than one fluorescent molecule in the observed volume.

Instrumentation. NR single molecule (SM) spectra embedded in polymer matrix were recorded with a home-built laser scanning confocal microscope,[28] (OSMP-Group, TU-Chemnitz). The sample was excited with linearly polarized laser light at 473 nm (DPSS Laser, Conoptics). The excitation power on the sample was 5 μW. The fluorescence signal was separated from the excitation light via a 502 nm long-pass filter (Omega Optical). The sample was scanned with a scanning mirror of a control stage (Newport). A 30:70 beam splitter allowed simultaneous recording of images with an avalanche photodiode (Perkin-Elmer) and SM spectra with a monochromator (300 lines/mm grating, Acton Research Corporation, SpectraPro 275) equipped with a liquid-nitrogen-cooled CCD camera (Princeton Instruments, ST-121). From the scanned image, locations of dye molecules were identified. At selected locations spectra were recorded with 1 s integration time. Time series of spectra were obtained by recording successive spectra at the same location. The simultaneous monitoring of spectrum and total emission intensity assured the observation of single molecules, since cases where photobleaching did not take place in one step were excluded from further analysis. In order to reduce photobleaching due to oxygen permeability and to control temperature, the sample was placed in a continuous flow cryostat (Janis Research-Model ST-500H) at 10^{-5} mbar. Objective Zeiss LD PLAN-NEOFLUAR 63× (NA = 0.75) was employed to take into account a correction due to the influence of the cryostat window thickness (0.5 mm). SM emission spectra in the energy domain were fitted well to a sum of up to four Gaussian shaped spectral lines. Data analysis was performed with our own Matlab written routines. Translational diffusion of NR was observed to be smaller than the confocal volume, within the observation time.

RESULTS AND DISCUSSION

Molecular positions were detected in scanned images obtained by confocal microscopy. From most of these identified spots, time series of spectra were obtained in a successive manner, shifting to another location after photobleaching occurred. Varying distributions of emission spectra were observed, not only in the different molecular locations but also as a result of local fluctuations. As described above, each spectrum was fitted to a sum of up to four Gaussian line shapes belonging to two realizations of fluorescence emission spectra with a fluorescence "origin" and a related (energetically nearly constant) vibrational sideband. The fluorescence origin was derived for each spectrum from the Gaussian line with the largest amplitude. This main emission peak wavelength was taken as a significant parameter to characterize the molecular environment. The energies of all these emission origins are displayed in Figure 1

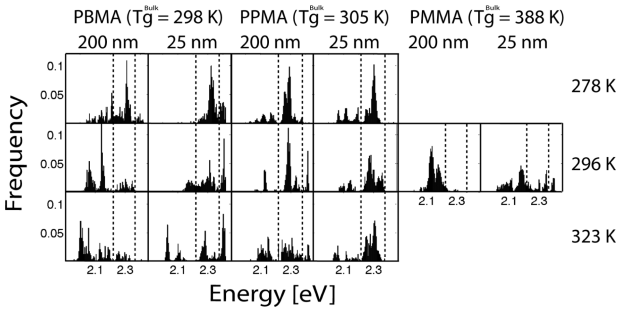

Figure 1. Frequency histograms of the energies of the emission maxima for all the registered and identified spectra of NR single molecules in PBMA (first and second column), PPMA (third and fourth column), and PMMA (fifth and sixth column) films of 25 and 200 nm (as indicated in each column) at three temperatures: 278 K (upper row), 296 K (middle row), and 323 K (bottom row). The frequencies are normalized to the number of molecules measured in each sample. Broken lines indicate the range of the fluorescence origin of the three configuration types A, B, and C (see the text).

as a frequency histogram for all spectra registered in the three polymers, for the two film thicknesses, and at three temperatures. The data compiled in Figure 1 have useful information regarding the type of spectra and the position of the emission maximum present in each medium. As will be discussed below, it contains the data to calculate the relative probability of exchangeable probe environments but lacks the time correlation information.

On the basis of the energy frequency histograms of Figure 1 and on the spectral distributions of Figure 2, the fluorescence emission spectra can be classified into three types (including fluorescence origin and vibrational sideband) according to the

dx.doi.org/10.1021/jp3004097 | J. Phys. Chem. C 2012, 116, 7573−7580

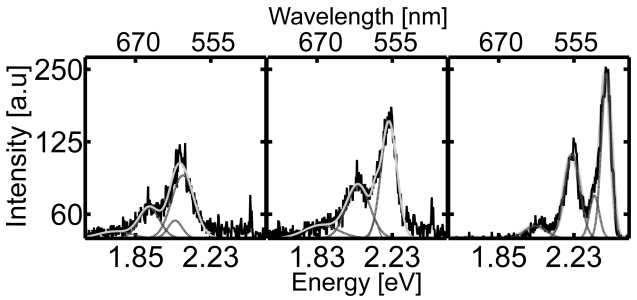

Figure 2. Example of three types of single molecule emission spectra of Nile Red embedded in a PBMA film of 200 nm thickness at 296 K. Typical cases of spectra of each type (1 s acquisition time) are shown (solid black line), as well as the corresponding fitted spectra obtained by a sum of four Gaussian shaped spectral lines (solid gray line; the individual components are shown as broken lines).

energy of the respective highest energy emission peak. The different types of spectra correspond to different probe polymer configurations.[25] They were classified and named as type A, those of the highest emission energy ($E \geq 2.37$ eV for the blue most emission maximum); type B, those of intermediate emission energy ($2.22\ \text{eV} \leq E \leq 2.37$ eV); and type C, those of the lowest maximum emission energy ($E \leq 2.22$ eV). The spectra are similar to the ones reported in the literature in PMMA[21] and polystyrene.[24] They were found in all the studied polymers. In PMMA films of 200 nm thickness at 296 K, the accumulated spectra of all measured single molecules matches the ensemble spectrum measured in a fluorometer at the same excitation wavelength, thickness, and temperature but, of course, different concentration (see Figure 1A in the Supporting Information). This fact means, on the one hand, that we are dealing with a representative single molecule ensemble in this case and, on the other hand, that these types of spectra are the only ones that contribute appreciably to the ensemble spectrum and are representative of the three different polymer environments where the probe locates. In general, the matching between the accumulated single molecule spectra and the steady state spectrum was not satisfactory (for a typical case, see Figure 1B in the Supporting Information). The main difference is the peak to the blue in the accumulated single molecule spectra, due to type A molecules, which are the brightest and most stable. These are not atypical molecules but are the ones that bias the statistic of total emission in single molecule experiments, which is a typical effect in these type of measurements. For this reason, a detailed quantitative analysis of distribution of spectral locations was not performed. Nevertheless, trends in the dependence of SM behavior on temperature and film thickness can be investigated by comparison of distributions of SM spectra obtained for varied experimental conditions.

The spectral positions obtained at the molecular locations can be compared to the spectral position of the dye in solution of different solvents to estimate the strength of the probe–polymer interactions in the cage. A table with literature values of the energy of the emission maximum of NR in different solvents is compiled in the Supporting Information. This analysis leads to the conclusion that type A environments are similar to hexane (peak at 2.36 eV[29]), while type B molecules fall in the range between CCl_4 (2.23[30]–2.25 eV[31]) and hexane and type C molecules locate in environments of interactions between CCl_4 and acetonitrile (1.98–2.03 eV[24,30,31]) or acetone (2.01–2.05 eV[30,31,32]). The probe can be accommodated in nonpolar environments, resembling hexane medium, if the alkyl chains face and surround the probe, keeping it apart from the ester groups. On the other hand, there are two ways in which the probe–polymer cage can resemble a polar environment. Either the ester groups can face the probe or it can be accommodated parallel to partially interdigitated alkyl chains so that the dimethylamino and carbonyl groups of NR are placed near the ester groups. These two probe moieties, where the charge separation locates, are the ones that predominate in the probe–polymer interactions (see Figure 3 in Supporting Information)

Figure 3 shows time traces of emission spectra for NR single molecules embedded in PBMA of 25 nm thickness at 323 K.

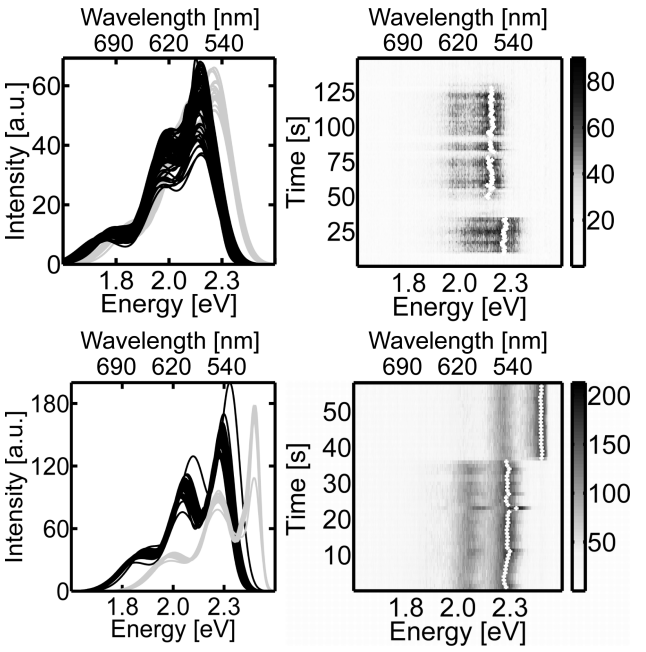

Figure 3. Two examples of time traces of SM emission spectra of NR embedded in a 25 nm thick PBMA film at 323 K. The different types of emission spectra are distinguished in gray scale, emission intensity (gray scale) as a function of time and energy (left). White dots represent the position of maximum emission in the fitted spectrum. (right).

Spectra were followed in time up to photobleaching. Time traces show distinct features. On one hand, a dominant small fluctuation of the emission energy is seen in successive spectra. The amplitude of these energy variations is on the order of a few millielectronvolts and can be assigned to small configurational changes, for example of the dimethylamino moiety of the dye or due to motion of lateral polymer groups. On the other hand, there are rarer cases of large energy variations (*jumps*) that are accompanied by a change of spectrum to another emission type, for example type B to type A or to type C. Such a case is observed in Figure 3 (bottom) at around 40 s. Before that time, the emission maximum is about 2.26 eV and fluctuates around the mean energy with a standard deviation of 0.008 eV. This corresponds to type B spectra. After ca. 40 s, the spectrum suddenly shifts to a state with higher emission energy (emission maximum at 2.39 eV) where it fluctuates less, with a standard deviation of 0.003 eV. Other SM spectra display the same pattern of frequent small fluctuations and rarer larger jumps together with photoblinking (Figure 3, top).

dx.doi.org/10.1021/jp3004097 | J. Phys. Chem. C 2012, 116, 7573–7580

Type A spectra are the most structured, the most stable upon light excitation, and brighter than the other two types of spectra. They display the smallest amplitude of spectral fluctuations, and they show the rarest spectral jumps. Type A molecules are related to a more stable and less polar cage compared to the others. On the other hand, type B and C spectra show more frequent photoblinking and are less intense than type A. The jumps normally occur between types B and C rather than between any one of them and type A. Due to the more frequent fluctuation between B and C type spectra, we combine those in the following analysis and separate them from type A.

To interpret the spectral fluctuations as a function of time, we simulate the time evolution of a two-level system with random fluctuations around a mean value and a low probability (measured in the exposure time interval scale) of performing a change between two configurations of different emission energy (characterized by the difference in the emission energy). The ratio of the probabilities per unit time to perform an upward or downward jump (k_{up} and k_{down}, respectively) is determined by the residence time in each level. Figure 4 displays simulations of the evolution of the maximum emission energy for such a system. The top plots display the energy of the emission maximum as a function of time. The time step was set to 1 s, equal to the exposure time in the spectral time evolution. Jump frequency (k_{up}, k_{down}), random noise, and difference in emission energy were varied to illustrate the influence of these parameters in the spectral time traces. We further characterize the spectral fluctuation of the probe emission by building the square of the energy difference between emission peaks of successive spectra (ΔE^2). In the bottom plots the logarithm of the complementary cumulative distribution function (CCDF) of ΔE^2, $\Phi_c(\Delta E^2)$, for each situation is shown for the simulated time traces. CCDF gives information about the probability that a random variable can have a value above a particular level, in this case, the square of the energy difference, ΔE^2.[29,33,34] The power of these types of plots resides in that, by presenting the data this way, we can unravel processes that might be otherwise buried in noise. In this respect it is similar to the analysis of intensity distribution in FCS,[35] where the highly emitting events, though rare, can be observed in the highest energy range of the distribution. In the center panel of Figure 4, $\Phi_c(\Delta E^2)$ of a real SM spectral behavior of one molecule is shown together with the best suited simulation (the time evolution behavior of the maximum energy is presented in Figure 4 of the Supporting Information). There are two distinct ranges in the plot of $\Phi_c(\Delta E^2)$. The steep slope at the origin is related to the small fluctuations around a mean value of energy corresponding to each stable state. The plateau is related to the energy jumps, which take place with a probability related to k_{up}, k_{down} and have mean absolute amplitude given by the value of ΔE^2 at which log Φ_c decreases 0.3 log units from the plateau value.

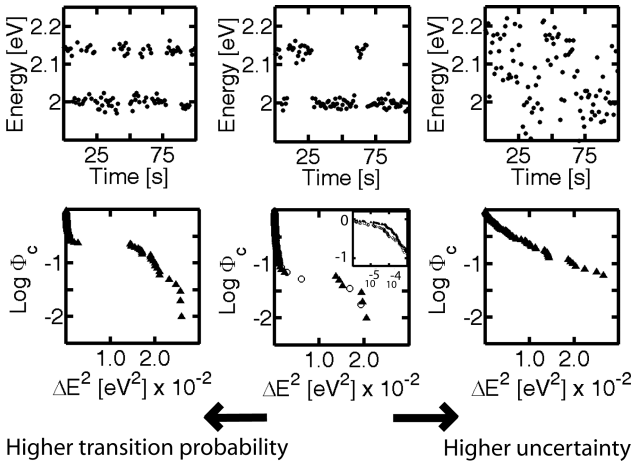

Figure 4. Simulation of the time evolution of the emission maximum energy of a system with two exchangeable energy levels. Spectral fluctuations can vary in energy, frequency, and uncertainty. Top plots show energy fluctuations with time and lower plots the resulting logarithm of the complementary cumulative distribution function, $\Phi_c(\Delta E^2)$ (see the text). The central lower panel displays, as full triangles, the Φ_c for a simulation for ΔE = 0.14 eV, a random noise of 0.012 eV, $k_{up} = k_{down}$ = 0.05 s^{-1} and, as hollow circles, a single molecule time trace (experimental values for a type C NR molecule in PBMA film of 200 nm thickness, T = 278 K; see also Figure 4 Supporting Information). In this same panel, the inset shows a detail of the lower ΔE^2 range in a double-log scale. Leftmost and rightmost lower panels illustrate extreme conditions of the center plot, increasing transition probability to $k_{up} = k_{down}$ = 0.3 s^{-1} (to the left) and noise amplitude to 0.05 eV (to the right).

As simulations show, an increase in the frequency of energy jumps leads to a higher $\Phi_c(\Delta E^2)$ in the plateau (left panel in Figure 4). When random noise is increased, approaching the absolute value of the energy variation, no jumps can be distinguished from the $\Phi_c(\Delta E^2)$ curves (right panel).

The picture of the fluctuations describing the behavior of one single molecule (Figure 4) acquires additional features when we enlarge the statistics by considering all the molecules of the same type in a given polymer, at a certain thickness and temperature. These results are depicted in Figure 5 for type A molecules in PBMA films of 25 nm thickness at 323 K and they are representative of the general behavior. The complete description of the spectral fluctuations has three components: (1) random very low amplitude fluctuations around a mean value that account for the great majority of the spectral fluctuations, (2) random fluctuations of larger amplitude also around a mean value, and (3) jumps of higher amplitude between two states of distinctive emission energy. The first component is attributed to the uncertainty of the fitting procedure. This component also includes fast fluctuations averaging to zero in the observation time window (1 s), such as thermal fluctuations. The second component can be ascribed to small conformational changes that also average to zero in the observation time window but have different values in the different locations even within the same type of spectra. This effect has been already observed.[29,34] The third component involves probe polymer conformational changes that can stabilize different ground and excited states of the probe with solvatochromic response on the order of magnitude of 0.1 eV. In the particular case of NR it might involve cage reorganization capable of stabilizing CT excited states of lower emitting energy. Changes in probe−polymer interactions that stabilize excited states of the probe with different photophysical features (e.g., excited state lifetime) have already been reported.[36,37]

A simulation of a time trace of the type described in the previous paragraph, obtained in the same way as the ones in Figure 4 but considering all three sources of spectral variation, is shown in Figure 5. Panel A shows Φ_c for type A spectra in PBMA films of 25 nm thickness at 323 K. Panel B shows the frequency histogram of ΔE values and panel C the fit of the low

dx.doi.org/10.1021/jp3004097 | J. Phys. Chem. C 2012, 116, 7573−7580

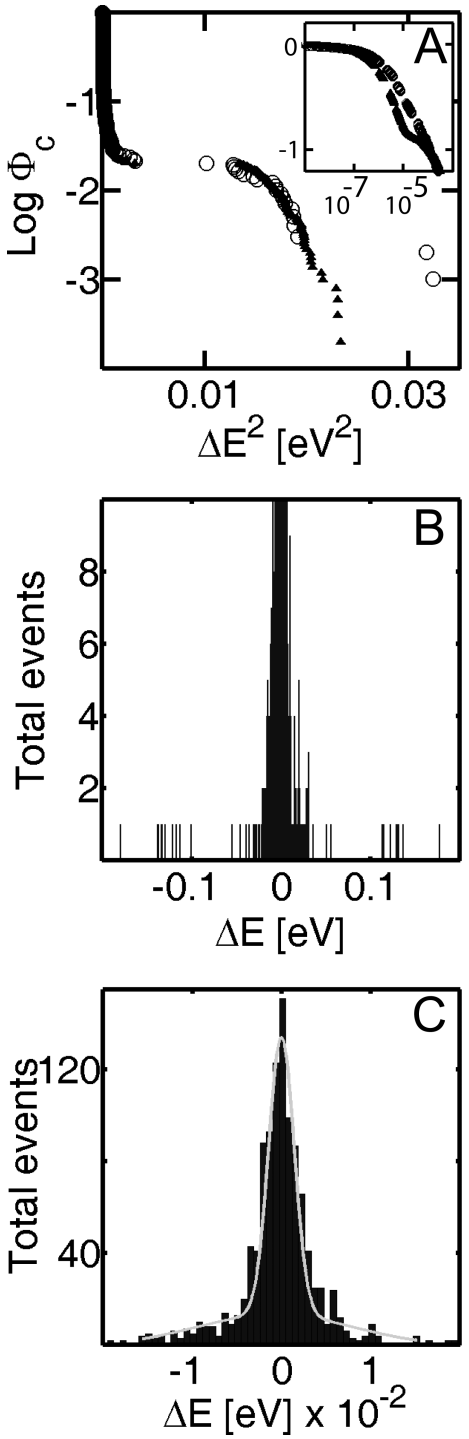

Figure 5. (A) Complementary cumulative distribution function for type A molecules of NR in PBMA films of 25 nm thickness at 323 K: hollow circles, experimental data; full triangles, simulation (see the text). The inset shows a detail of the lower ΔE^2 range in a double-log scale. (B) Histogram of energy differences between successive spectra. (C) Fit of the central part of the histogram in part B to a sum of two Gaussian functions. The result of this fit is $(94 \pm 4)\ \exp\{-(\Delta E^2/[2 \times (1.9 \pm 0.2) \times 10^{-3}\ \text{eV}]^2)\} + (12 \pm 3)\ \exp\{(\Delta E^2/[2 \times (8.2 \pm 0.9) \times 10^{-3}\ \text{eV}]^2)\}$.

absolute value ΔE fluctuations by a sum of two Gaussian functions. In this fit, it is not possible to include the large amplitude variations due to their small contribution to the overall distribution, but their presence is evident by the two small accumulations of events, symmetrically distributed at 0.13 and −0.13 eV, shown in panel B. From the Gaussian fits, the standard deviation of the two types of fluctuations with a mean value of zero can be obtained. For this particular case, these values are $(1.9 \pm 0.2) \times 10^{-3}$ eV as standard deviation for the smallest amplitude fluctuations and $(8.2 \pm 0.9) \times 10^{-3}$ eV for the larger amplitude fluctuations around a mean value of zero. By a simulation to the total data set displayed in panel A, the higher amplitude energy differences can be determined to be of 0.13 ± 0.01 eV. Panel A of Figure 5 shows this simulation as full triangles, including all three components. The agreement with the experimental data is satisfactory.

Figure 6 shows $\Phi_c(\Delta E^2)$ of type B and C spectra of NR in PBMA and PPMA films of 25 and 200 nm thickness. It can be

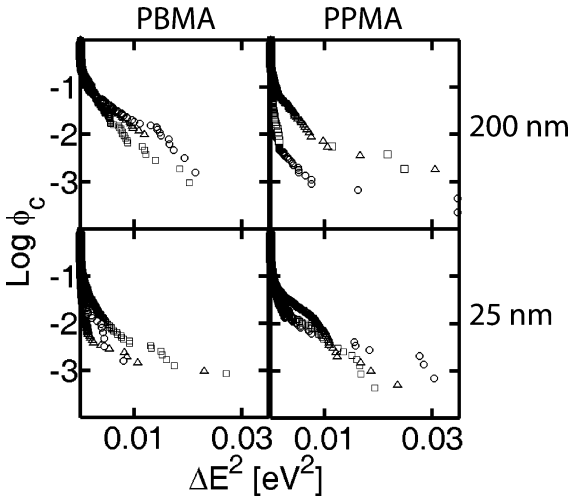

Figure 6. Semilogarithmic plots of complementary cumulative distributions of type B and C SM spectral fluctuations of NR embedded in PBMA (left column) and PPMA (right column) of 200 and 25 nm thickness: circles, 278 K; squares, 296 K; triangles, 323 K .

seen that the large amplitude fluctuations are more frequent for B + C spectra in 200 nm films than in the 25 nm ones for both PPMA and PBMA. Type A molecules display jumps with an average absolute amplitude of 0.12 eV with 3% probability only in 25 nm thick PBMA at 323 K; in the other polymers or in PBMA at lower temperature, type A molecules display 0.12 eV jumps with less than 1% probability [$\Phi_c(\Delta E^2)$ of type A molecules are displayed in Figure 5 Supporting Information]. Due to the low probability of these events, they do not contribute significantly to the large amplitude energy variations responsible for the plateau of the distribution functions of SM spectra presented in Figure 6. Type A environments are less polar and resemble alkane-like medium. Nile Red emission quantum yield (ϕ_f) is enhanced in nonpolar environments compared to polar ones; for example, $\phi_f = 0.65$ in CCl_4, 0.33 in chloroform, 0.32 in acetone, 0.29 in acetonitrile, and 0.08 in methanol.[28,38]

It is well-documented that a film thickness below about 100 nm affects T_g. Around T_g the persistence length of the collective motion of the polymer chains increases and approaches the thickness of thin films, causing a shift in T_g.[39,40] Changes in T_g up to 30 °C have been reported for such thin films compared to thick ones (micrometer range).[24,40−42] In a systematic work of poly(alkyl methacrylates) on silica slides,[43] the authors find that the magnitude and sign of the

dx.doi.org/10.1021/jp3004097 | J. Phys. Chem. C 2012, 116, 7573−7580

difference between the bulk and the thin film T_g depends on the polymer, on the thickness of the film, and on the interface of the polymer film (polymer/glass or polymer/air). This work shows no T_g difference for 200 nm films, whereas in 25 nm films, they measure an increase of 6 °C for PMMA and a decrease of ca. 18 °C for PPMA, while no change is observed for PiBMA in all cases compared to the bulk T_g. No measurements on PBMA were performed. This work reports the conditions that most closely match our samples. A research of PS and PMMA thin films (18−80 nm thick) on substrates of different surface energy shows a linear correlation between the difference in T_g and the surface energy of the substrate.[44] At low surface energy, a decrease in T_g is measured for both polymers in the film with respect to bulk, and this situation is reverted upon increasing the surface energy. The competing effects of adhesion and polymer cohesive interactions can result in compensating effects that do not change the film T_g.[45,46] In all the mentioned cases, either dynamic properties of the film or total fluorescence emission from a probe was measured. Clearly collective dynamics is influenced by T_g, but the spectral changes monitored in our work might only be determined by a conformational change of a moiety either of the probe or of the polymer located in special positions of the cage, for example, the approximation of the carbonyl functionality of the polymer and the carbonyl or diethylamino groups of the probe. The present work shows that there is a poor correlation of the amplitude and frequency of the spectral fluctuations of NR with the nature of the polymer or the film thickness. Moreover, in spite of the strong medium sensitivity of NR, there are larger variations in spectra between different locations within the same polymer sample than between different polymers (or any other change in conditions). This result may suggest that spectral fluctuations are not related to glass transition temperature but to van der Waals interactions between components of the cage walls and relaxation of the alkyl and ester groups that start rotating at very low temperature.[47,12] The rates of segmental relaxation phenomena near the probe molecules are loose enough and do not experience large temperature variations in the range studied. As these groups are the same in all the polymers, this can explain the similarities observed in the behavior of NR spectra. Considering the homogeneity of the results under all the conditions, we prefer this explanation.

The energy difference of 0.13 ± 0.01 eV can be translated into a change in the cage characteristics if we use a solvatochromic plot, correlating the emission energy maximum of NR with empirical solvent scales (see Supporting Information, Figure 2). Considering type A molecules to be located in hexane type environments (2.39 eV emission maximum), a decrease in 0.13 eV in the emission energy shifts the value to that corresponding to carbon tetrachloride (2.25 eV). Mean amplitude spectral jumps of 0.13−0.15 eV are observed in all cases. For type B molecules this will mean a shift from an environment close to carbon tetrachloride to values similar to ethyl acetone, chloroform, or tetrahydrofuran. The fact that the amplitude of the large energy jumps is very similar for all polymer films points to a similar feature responsible for this type of fluctuation in all cases. We postulate that the motion of the side groups of the polymer chain is responsible for the interaction changes, especially the carbonyl group present in all polymers. This conclusion was also found for the interaction of pyrenyl groups in poly(alkylmethacrylate) films.[48]

Finally, we can analyze the time information of the spectral evolution. To perform this, we build an artificial time trajectory by assembling one after the other all time traces of molecules of the same emission type in each polymer sample at a given thickness and temperature. The ordering of the assembling is irrelevant as we will only compute the total number of spectra (frames) with energy at the emission maximum above and below a certain energy threshold. The number of spectra (frames) is equivalent to a residence time because all frames were acquired using the same exposure time. Type A emission, on one hand, and type B + C emission, on the other hand, are distinguished (Figure 6 in the Supporting Information shows one such trajectory for type A molecules in 25 nm PBMA films at 323 K). Molecules spend more than 99% of the time as type A, with a small probability of changing to other type of emission (mostly type B). The case for B + C is more meaningful, as shown by Figure 7 A. We define an equilibrium

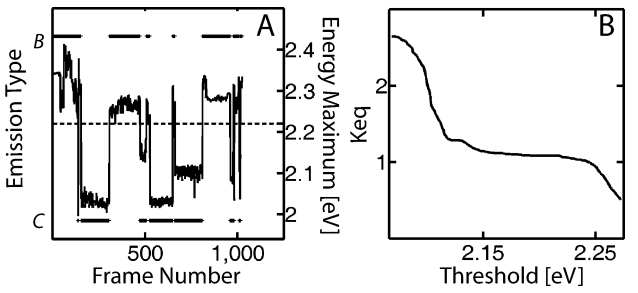

Figure 7. (A) Position of the emission maximum in successive frames of all the type B and C spectra of the group of molecules measured in a 25 nm thick film of PBMA at 323 K and the corresponding discrimination in B or C type emission with 2.22 eV as the threshold value (broken horizontal line). (B) Value of the calculated K_{eq} as a function of the threshold value between B and C.

constant K_{eq} between the probe−polymer cage conformations responsible for the different spectral emission as $K_{eq} = t_B/t_C$, where $t_{B,C}$ is the total time the molecules emit as type B or C, respectively. The emission type is distinguished by the energy threshold between the configurations. Figure 7B displays the value of the calculated K_{eq} as a function of the threshold value between B and C. For all polymers, temperatures, and film thickness, the threshold was set to 2.22 eV, in agreement with the criterion used to distinguish type B from type C emission. The values of K_{eq} are summarized in Table 1. In PBMA the values of K_{eq} decrease with increasing temperature. In PPMA the variation is much milder, showing almost constant values. Considering the values of K_{eq} in Table 1, two quantitative results stand out. The first is the high value of K_{eq} in 25 nm

Table 1. Value of the Equilibrium Constant K_{eq} for Spectral Configuration Changes C → B Emission Types in PBMA and PPMA at Different Temperatures and Film Thicknesses

	25 nm			200 nm		
	278 K	296 K	323 K	278 K	296 K	323 K
			PBMA			
K_{eq}	10^2	2.3	1.1	1.7	0.3	0.2
ΔH(kJ/mol)		−70 ± 35			−34 ± 15	
ΔS (J/K mol)		(−2.2 ± 1.1) × 10^2			(−1.2 ± 0.6) × 10^2	
			PPMA			
K_{eq}	2.2	3.8	3.4	3.3	3.3	1.0

dx.doi.org/10.1021/jp3004097 | J. Phys. Chem. C 2012, 116, 7573−7580

PBMA films at 278 K and the second is the difference in the temperature dependence of K_{eq} between PBMA (exothermic) and PPMA (almost invariant with temperature). The first result can be due to the low frequency of type C spectra in PBMA under the mentioned conditions. This can be also seen from Figure 1, where it is evident that the occurrence of type C spectra increases much faster with rising temperature in PBMA than in PPMA. The B to C transition in PBMA has the thermodynamic characteristics of a melting process: rising in entropy and in energy. A possible interpretation can be to postulate that C locations in PBMA require a melting of the butyl chains in order that the probe can approach the carbonyl moieties better. This situation could be different in PPMA because B to C transition might only require a shift in the probe location to slightly approach the ester groups without rearrangement of the alkyl chains. The different conformations of the polar cages can be due to the different alkyl chain length (see Figure 3 of the Supporting Information).

CONCLUSIONS

Spectral fluctuations in poly(alkyl methacrylate) films could be measured by single molecule emission spectroscopy. The fluctuations of larger amplitude (more than 0.1 eV) arise in probe−polymer cage conformational changes that stabilize Nile Red emission states of charge transfer character. These types of changes are very similar in the three studied polymers and do not vary either with film thickness in the 25−200 nm range or with temperature in the 278−323 K range. The similarity of behavior points to a common probe−polymer interaction change as responsible for the fluctuations: complex cage rearrangements, involving the carbonyl moiety of the polymer as the common actor are postulated to be the cause of the largest amplitude spectral fluctuations. We assign type A spectra to nonpolar and type B and C spectra to polar cages. The discrimination between polar and nonpolar cages is supported by the spectral linewidths, which is broader for type B and C spectra as compared to type A ones.

ASSOCIATED CONTENT

Supporting Information

Comparison of bulk and accumulated single molecule emission spectra of Nile Red, table with summary of literature information on the emission solvatochromism of Nile Red in different solvents as well as a plot of the emission maxima as a function of Reichardt's ET(30) solvation scale, schematic representations of polar and nonpolar environments for NR in PBMA or PPMA time trace of the single molecule exemplified in Figure 4, complementary cumulative distribution function for type A molecules, and emission time trace for a type A molecules. This material is available free of charge via the Internet at http://pubs.acs.org.

AUTHOR INFORMATION

Corresponding Author

*E-mail: borczyskowski@physik.tu-chemnitz.de (C.v.B.), pedro@qi.fcen.uba.ar (P.F.A.).

Notes

The authors declare no competing financial interest.

ACKNOWLEDGMENTS

B.A. is a Doctoral Fellow and P.F.A. is Research Staff from Consejo Nacional de Investigaciones Científicas y Técnicas (CONICET, Argentina). We thank DAAD (Germany)-MINCyT (Argentina) for a Research Collaboration grant (DA-0807). The work was performed under support from grants PICT 06-34193 (ANPCyT), UBA-X006, and PIP 5470 (CONICET), all three from Argentina. Support within the DFG-SFG 877 is gratefully acknowledged. We thank D. R. T. Zahn, (CUT) for the use of the ellipsometry equipment, Danny Kowerko (CUT) for provision of the Matlab program for fitting spectra, and Stefan Krause (CUT) for support concerning the use of the confocal microscope and for improvement of the Matlab program

REFERENCES

(1) Matharu, A. S; Jeeva, S.; Ramanujam, P. S. *Chem. Soc. Rev.* **2007**, *36*, 1868−1880.
(2) Yu, Y.; Ikeda, T. *J. Photochem. Photobiol. C: Photochem. Rev.* **2004**, *5*, 247−265.
(3) Finkelmann, H.; Nishikawa, E.; Pereira, G. G.; Warner, M. *Phys. Rev. Lett.* **2001**, *87*, 015501−015505.
(4) Richert, R. *J. Phys. Chem. B* **1997**, *101*, 6323−6326.
(5) Richert, R.; Heuer, A. *Macromolecules* **1997**, *30*, 4038−4041.
(6) Wei, C. Y. J.; Kim, Y. H.; Darst, R. K.; Rossky, P. J.; Vanden Bout, D. A. *Phys. Rev. Lett.* **2005**, *95*, 17300:1−17300:4.
(7) Adhikari, A. N.; Capurso, N. A.; Bingemann, D. *J. Chem. Phys.* **2007**, *127*, 114508:1−114508:9.
(8) Krause, S.; Kowerko, D.; Boerner, C.; Huebner, C. G.; von Borczyskowski, C. *ChemPhysChem* **2011**, *12*, 303−312.
(9) Garcia-Parajo, M. F.; Veerman, J. A.; Bouwhuis, R.; Vallee, R.; van Hulst, N. F. *ChemPhysChem* **2001**, *2*, 347−360.
(10) Kumbhakar, M.; Nath, S.; Mukherjee, T.; Mittal, J. P.; Pal, H. *J Photochem. Photobiol. C* **2004**, *5*, 113−137.
(11) Wustholz, K. L.; Sluss, D. R. B.; Kahr, B.; Reid, P. J. *Int. Rev. Phys. Chem.* **2008**, *27*, 167−200.
(12) Wöll, D.; Braeken, E.; Deres, A.; De Schryver, F. C.; Uji-i, H.; Hofkens, J. *Chem. Soc. Rev.* **2009**, *38*, 313−328.
(13) Lupton, J. M. *Adv. Mater.* **2010**, *22*, 1689−1721.
(14) Wang, H. M.; Bardo, A. M.; Collinson, M. M.; Higgins, D. A. *J. Phys. Chem. B.* **1998**, *102*, 7231−7237.
(15) Biju, V. P.; Ye, J. Y.; Ishikawa, M. *J. Phys. Chem. B.* **2003**, *107*, 10729−10735.
(16) Vallee, R.; Tomczak, N.; Gersen, H.; van Dijk, E.; Garcia-Parajo, M. F.; Vancso, G. J.; van Hulst, N. F. *Chem. Phys. Lett.* **2001**, *348*, 161−167.
(17) Wei, C. Y. J.; Vanden Bout, D. A. *J. Phys. Chem. B* **2009**, *113*, 2253−2261.
(18) Wei, C. Y. J.; Lu, C. Y.; Kim, Y. H.; Vanden Bout, D. A. *J. Fluoresc.* **2007**, *17*, 797−804.
(19) Dickson, R. M.; Norris, D. J.; Tzeng, Y. L.; Sakowicz, R.; Goldstein, L. S. B.; Moerner, W. E. *Mol. Cryst. Liq. Cryst.* **1996**, *291*, 31−39.
(20) Hou, Y. W.; Bardo, A. M.; Martinez, C.; Higgins, D. A. *J. Phys. Chem. B.* **2000**, *104*, 212−219.
(21) Hou, Y. W.; Higgins, D. A. *J. Phys. Chem. B* **2002**, *106*, 10306−10315.
(22) Higgins, D. A.; Collinson, M. M.; Saroja, G.; Bardo, A. M. *Chem. Mater.* **2002**, *14*, 3734−3744.
(23) Kim, H. H.; Song, N. W.; Park, T. S.; Yoon, M. *Chem. Phys. Lett.* **2006**, *432*, 200−204.
(24) Kawski, A.; Bojarski, P.; Kuklinski, B. *Chem. Phys. Lett.* **2008**, *463*, 410−412.
(25) Viseu, T. M. R.; Hungerford, G.; Coelho, A. F.; Ferreira, M. I. C. *J. Phys. Chem. B* **2003**, *107*, 13300−13312.
(26) Dutta, A. K.; Kamada, K.; Ohta, K. *J. Photochem. Photobiol. A: Chem.* **1996**, *93*, 57−64.
(27) Jee, A.-Y.; Park, S.; Kwon, H.; Lee, M. *Chem. Phys. Lett.* **2009**, *477*, 112−115.
(28) Krause, S.; Aramendía, P. F.; Täuber, D.; von Borczyskowski, C. *Phys. Chem. Chem. Phys.* **2011**, *13*, 1754−1761.

(29) Boldrini, B.; Cavalli, E.; Painelli, A.; Terenziani, F. *J. Phys. Chem. A* **2002**, *106*, 6286−6294.
(30) Ghanadzadeh Gilani, A.; Moghadam, M.; Zakerhamidi, M. S. *Dyes Pigm.* **2012**, *92*, 1052−1057.
(31) Sackett, D. L.; Wolff, J. *Anal. Biochem.* **1987**, *167*, 228−234.
(32) Greenspan, P; Fowler, S. D. *J. Lipid Res.* **1985**, *26*, 781−789.
(33) Hellriegel, C.; Kirstein, J.; Bräuchle, C.; Latour, V.; Pigot, T.; Olivier, R.; Lacombe, S.; Brown, R.; Guieu, V.; Payaraste, T.; Izquierdo, A.; Mocho, P. *J. Phys. Chem. B* **2004**, *108*, 14699−14709.
(34) Täuber, D. Dissertation, TU Chemnitz, 2011.
(35) Muller, J. D.; Chen, Y.; Gratton, E. *Biophys. J.* **2000**, *78*, 474−486.
(36) Vallée, R. A. L.; Marsal, P.; Braeken, E.; Habuchi, S.; De Schryver, F. C.; Van der Auweraer, M.; Beljonne, D.; Hofkens, J. *J. Am. Chem. Soc.* **2005**, *127*, 12011−12020.
(37) Braeken, E.; Marsal, P.; Vandendriessche, A.; Smet, M.; Dehaen, W.; Vallée, R. A. L.; Beljonne, D.; Van der Auweraer, M. *Chem. Phys. Lett.* **2009**, *472*, 48−54.
(38) Ghoneim., E. *Spectrochim. Acta A* **2000**, *56*, 1003−1010.
(39) Ellison, C. J.; Torkelson, J. M. *Nat. Mater.* **2003**, *2*, 695−700.
(40) Keddie, J. L.; Jones, R. A. L.; Cory, R. A. *EPL (Europhys. Lett.)* **1994**, *27*, 59−64.
(41) Mundra, M. K.; Ellison, C. J.; Rittigstein, P.; Torkelson, J. M. *Eur. Phys. J. ST* **2007**, *141*, 143−151.
(42) Kim, S.; Roth, C. B.; Torkelson, J. M. *J. Polym. Sci. Part B, Polym. Phys* **2008**, *46*, 2754−2764.
(43) Priestley, R. D.; Mundra, M. K.; Barnett, N. J.; Broadbelt, L. J.; Torkelson, J. M. *Aust. J. Chem.* **2007**, *60*, 765−771.
(44) Fryer, D. S.; Peters, R. D.; Kim, E. J.; Tomaszewski, J. E.; De Pablo, J. J.; Nealey, P. F.; White, C. C.; Wu, W.-L. *Macromolecules* **2001**, *34*, 5627−5634.
(45) Forrest, J. A.; Dutcher, J. R. *Phys. Rev. E* **1997**, *56*, 5705−5716.
(46) Richert, R. *Annu. Rev. Phys. Chem.* **2011**, *62*, 65−84.
(47) Yoshii, K.; Machida, S.; Horie, K. *J. Polym. Sci. Part. B: Polym. Phys.* **2000**, *38*, 3098−3105.
(48) Abraham, S.; Atvars, T. D. Z.; Weiss, R. G. *J. Phys. Chem. B.* **2010**, *114*, 12221−12233.